Available online at www.sciencedirect.com
ScienceDirect
Journal of Power Sources 171 (2007) 1023–1032
JOURNAL OF POWER SOURCES
www.elsevier.com/locate/jpowsour

Dynamic electrochemical model of an alkaline fuel cell stack

Matthias Duerr*, Sinclair Gair, Andrew Cruden, Jim McDonald

Centre for Economic Renewable Power Delivery, University of Strathclyde, 204 George Street, Glasgow G1 1XW, United Kingdom

Received 28 November 2006; received in revised form 25 May 2007; accepted 3 June 2007
Available online 16 June 2007

Abstract

The Institute for Energy and Environment (IEE) at the University of Strathclyde has developed various fuel cell (FC) systems for stationary and vehicular applications. In particular the author is involved in the development of alkaline fuel cell (AFC) systems. To understand the dynamic behaviour of the system's key element, the alkaline fuel cell stack, a dynamic model was developed allowing the characterisation of the electrochemical parameters. The model is used to forecast the behaviour of the fuel cell stack under various dynamic operating conditions. The so-called Nernst potential, which describes the open circuit voltage of the stack, is calculated using thermodynamic theory. Electrochemistry theory has been used to model the sources of the electric losses within the FC, such as activation, ohmic and concentration losses. The achievable value of this paper is the first publication of a detailed dynamic AFC based on mass balance, thermodynamics and electrochemical theory. The effects of the load changes on various fuel cell parameters, such as electrolyte concentration and concentrations of dissolved hydrogen and oxygen were covered in this investigation using the author's model. The model allows a detailed understanding of the dynamic effects within the AFC during load change events, which lead to the experienced electric response of the overall FC stack.

Keywords: Fuel cells; Modelling; Alkaline; Dynamic

1. Introduction

The Centre of Economic Renewable Power Delivery (CERPD) at the University of Strathclyde has developed various fuel cell (FC) systems for stationary and vehicular applications over the last 5 years. The aim of the research is the design and build of reliable and cost efficient hybrid FC/battery systems, which could replace existing conventional technology in the near future. A domestic scale combined heat and power (CHP) alkaline fuel cell (AFC) system has been developed. The small AFC stack (1–3 kW_e) is used to satisfy the average load demand of the domestic load profile of a stationary application. Whereas the load peaks are supplied by a battery system working in parallel with the AFC stack.

However, using an AFC for a highly fluctuating domestic load needs precise knowledge of the dynamic behaviour of the fuel cell system and consequently of its main component, the fuel cell stack. This paper describes a dynamic electrochemical model of an alkaline fuel cell stack. The practical electric losses of the fuel cell, such as activation, ohmic and concentration losses are considered and the variations of internal fuel cell parameters, such as reactant concentrations and pressures, during steady-state operation and dynamic load changes are shown and explained.

2. AFC operation

An AFC operates by introducing hydrogen and oxygen (in case of the modelled Zetek stack provided as air) gases into the gas diffusion layers of the anode and cathode, respectively. The gases subsequently diffuse into the catalyst layers of the electrodes, where they partly dissolve into the KOH electrolyte. To avoid gases entering the electrolyte layer the potassium hydroxide solution (KOH) in the electrolyte compartment has a slightly higher pressure than the gases in the anode and cathode. The normal operating pressure of hydrogen and air for the FC were set to 40 mbar above atmospheric pressure, whereas the KOH pressure is set to 100–150 mbar. The oxidation reaction occurring in the catalytic layer of the anode causes the hydrogen to decompose and yields electrons to the current collector and the remaining protons react with the hydroxyl ions available in the KOH solution [1].

* Corresponding author. Tel.: +44 141 548 4711; fax: +44 141 548 4872.
E-mail address: m.duerr@eee.strath.ac.uk (M. Duerr).

0378-7753/$ – see front matter © 2007 Elsevier B.V. All rights reserved.
doi:10.1016/j.jpowsour.2007.06.011

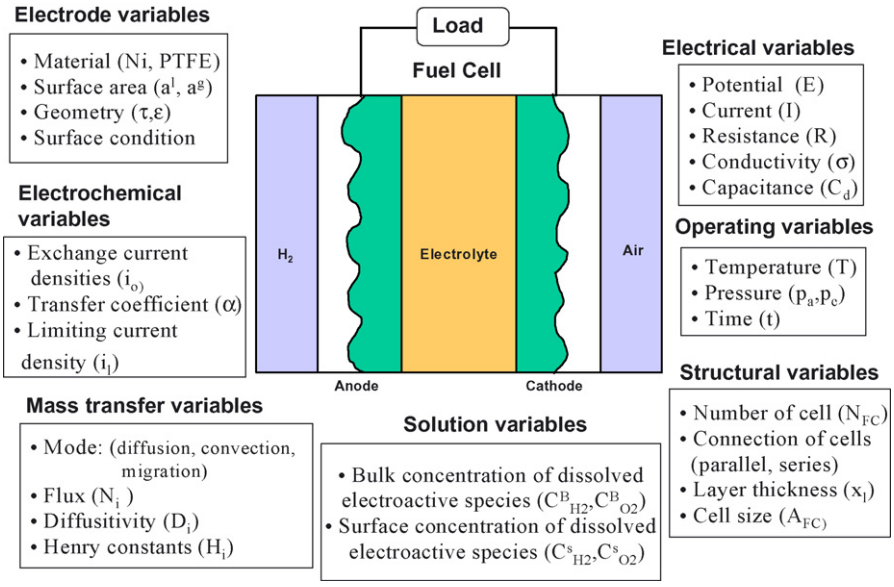

Fig. 1. Variables affecting the dynamic behaviour of an AFC stack.

At the cathode, the catalytic reduction of oxygen with water of the electrolyte and electrons supplied from the anode, to generate hydroxyl ions. The electro-osmotic drag within the cell, the electrolyte concentration gradient and the movement of charge particles in the electric field, moves the hydroxyl ions towards the anode. The electrode reactions as explained are given in the following equations:

$$H_2 + 2(OH^-) \rightarrow 2H_2O + 2e^- \quad (1)$$

$$H_2O + 0.5O_2 + 2e^- \rightarrow 2(OH^-) \quad (2)$$

Hence, the overall reaction of the fuel cell can be expressed as

$$H_2 + 0.5O_2 \rightarrow H_2O \quad (3)$$

3. The AFC stack model

The AFC behaviour is complex and is influenced by a large number of parameters. The model parameters can be grouped into four categories:

(1) *Operating parameters*: such as gas inlet pressures and temperature, reference electrolyte concentration.
(2) *Electrochemical parameters*: such as exchange current density of the electrodes, transfer coefficients of oxidation and reduction processes.
(3) *Material parameters*: such as composition of the electrodes and the current collectors, porosity of the materials, conductivity of electrodes.
(4) *Structural parameters*: such as layer thicknesses, active area sizes, number of cells.

Fig. 1 shows a summary of the most important fuel cell variables, which influence the dynamic stack performance.

The detailed model developed is based on a combination of the variables and parameters shown in Fig. 1, which are related through mass balance, mass transfer theory, thermodynamics, electrochemical and electrical theories [2].

For the purpose of analysis the alkaline fuel cell was split into five layers, each of which was modelled separately. These layers are:

- anode gas diffusion layer;
- anode catalyst layer;
- electrolyte layer;
- cathode catalyst layer;
- cathode gas diffusion layer.

Within each layer the appropriate state parameters, e.g. the partial pressures of the gases within the diffusion layers, the concentrations of the reactant species within the catalyst layer, were determined. The different layers are linked through input and output parameters. The modelled single cell performance was scaled according to the number of cells in the stack. It was assumed that all cells in the stack behave in a similar way. The physical structure of the AFC and a schematic of the top layer of the fuel cell model are shown in Figs. 2 and 3, respectively.

The model has been developed within the simulation package Matlab/Simulink. The block diagram shows the sub-systems of the anode and cathode gas diffusion layers, the anode and cathode catalyst layers and the electrolyte layer in the middle. The input parameter of the fuel cell stack model is the load current demand I_{load}. The main output parameter is the FC stack voltage E_{stack}.

3.1. Model equations

3.1.1. Gas diffusion layers

Each electrode possesses a gas diffusion layer, which is necessary to provide the process gases uniformly and extract the

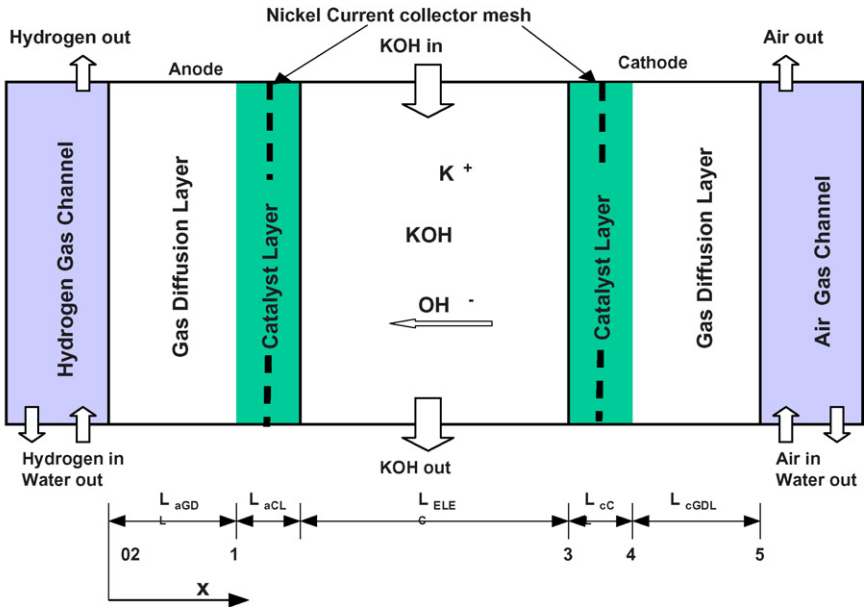

Fig. 2. Layer structure of the alkaline fuel cell.

product species. They are designed to prevent the electrolyte from weeping into the gas stream. Consequently, the model assumes that the hydrophobicity of the electrode will prevent any liquid from entering this region. Therefore, only hydrogen gas and water vapour will exist in the anode gas diffusion layer, and oxygen gas, nitrogen gas and water vapour will exist in the cathode gas diffusion layer.

The diffusion gas transport through porous material is described by the one-dimensional Stefan–Maxwell diffusion equation:

$$\frac{\mathrm{d}y_i}{\mathrm{d}x} = \sum_j \frac{RT}{pD_{ij}^{\mathrm{g}}}(y_i N_j - y_j N_i) \tag{4}$$

The list of symbols is given in Appendix A. To describe the mass balance in the gas diffusion layer the continuity equation has been used. The general one-dimensional continuity equation

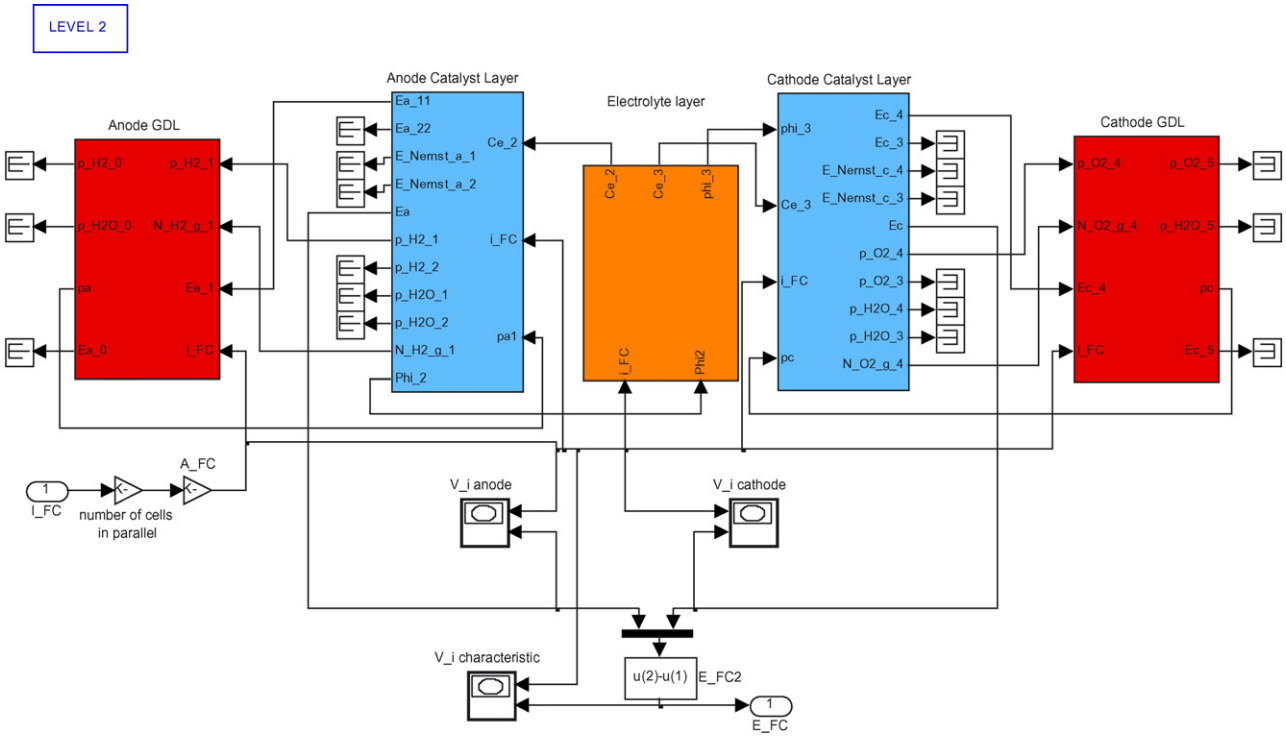

Fig. 3. The detailed alkaline fuel cell model.

is given by the following equation:

$$\frac{1}{RT}\frac{\mathrm{d}\varepsilon^{\mathrm{GDL}}p_i}{\mathrm{d}t} = -\frac{\mathrm{d}N_i}{\mathrm{d}x} + R_i^{\mathrm{p}} + R_i^{\mathrm{e}} \tag{5}$$

Within the gas diffusion layer there occurs no chemical reaction and no mass transport across a phase boundary (from gas to liquid or reverse), hence R_i^{p} and R_i^{e} equals zero. The continuity equation becomes:

$$\frac{1}{RT}\frac{\mathrm{d}\varepsilon^{\mathrm{GDL}}p_i}{\mathrm{d}t} = -\frac{\mathrm{d}N_i}{\mathrm{d}x} \tag{6}$$

The anode contains two species, hydrogen and water, whereas the cathode is assumed to contain oxygen, nitrogen and water.

3.1.2. Catalyst layers

The mass balances on anode and cathode are defined by the one-dimensional continuity equation. In the catalyst layers the reaction gases hydrogen and oxygen dissolve into the liquid electrolyte. The rate that the hydrogen and oxygen gases dissolve in the electrolyte is expressed by the mass transport rate over the phase boundary R_i^{p}. In equilibrium the transport of species i across the phase boundary, i.e. the amount of gases dissolved in the liquid electrolyte, can be described as follows

$$R_i^{\mathrm{p}} = -\frac{\mathrm{d}N_i^{\mathrm{p}}}{\mathrm{d}x} = -a^{\mathrm{g}}D_i^{\mathrm{l}}\left(\frac{H_i p_i - C_i}{\delta}\right) \tag{7}$$

The amount of oxygen and hydrogen that react in the catalyst layer is expressed with the electrochemical reaction rate R_i^{e}. The reaction interface area is not equal to the contact area of the CL and electrolyte layer; it is rather defined by the area where the electrolyte is in contact with the active material within the catalyst layer. This reaction area is expressed through a^{l} the specific area of catalyst–electrolyte interface. The reaction rate can be represented with Faraday's law:

$$R_i^{\mathrm{e}} = -\frac{\mathrm{d}N_i^{\mathrm{e}}}{\mathrm{d}x} = -\frac{s_i a^{\mathrm{l}} i^{\mathrm{loc}}}{z_i F} \tag{8}$$

The gas transport is modelled using the Stefan–Maxwell equation for gas diffusion in porous material (Eq. (5)) and the mass transport of the liquid species was described by the one-dimensional Nernst–Plank equation:

$$N_i^{\mathrm{l}} = -D_i^{\mathrm{l}}\frac{\mathrm{d}C_i}{\mathrm{d}x} - z_i u_i F C_i \frac{\mathrm{d}\Phi}{\mathrm{d}x} - C_i \upsilon^{\mathrm{ave}} \tag{9}$$

The reactants on anode and cathode diffuse, in gaseous form, through the 'dry' part of the catalyst layer, dissolve in the liquid electrolyte and react as stated in Eqs. (1) and (2) on the interface area within the catalyst layer. The electrochemical potentials of anode and cathode have been described by the Nernst equation. Included in the model is the used current–overpotential equation which takes into consideration the electric losses under load conditions (including the transport losses):

$$E^{\mathrm{N}} = E^{\mathrm{N},0} - \frac{RT}{z_i F}\ln\left[\prod\left(\frac{C_i}{C_i^{\mathrm{ref}}}\right)^{s_i}\right] \tag{10}$$

$$i^{\mathrm{loc}} = i_0^{\mathrm{loc}}\left[\prod_i\left(\frac{C_i}{C_i^{\mathrm{ref}}}\right)^{q_i} \mathrm{e}^{\alpha a F\eta/RT} - \prod_j\left(\frac{C_j}{C_j^{\mathrm{ref}}}\right)^{q_j} \mathrm{e}^{-\alpha c F\eta/RT}\right] \tag{11}$$

In the model Eq. (11) was expressed in the form of the Tafel equation. Thus, the anode and cathode overpotentials are respectively:

$$\eta_{\mathrm{a}} = \frac{2.303RT}{z_{\mathrm{a}}\alpha_{\mathrm{a}}F}\left(\log i_{\mathrm{a}}^{\mathrm{loc}} - \log i_{0,\mathrm{a}}^{\mathrm{loc}} - \log\left[\prod_i\left(\frac{C_i}{C_i^{\mathrm{ref}}}\right)^{q_i}\right]\right) \tag{12}$$

$$\eta_{\mathrm{c}} = -\frac{2.303RT}{z_{\mathrm{c}}\alpha_{\mathrm{c}}F}\left(\log i_{\mathrm{c}}^{\mathrm{loc}} - \log i_{0,\mathrm{c}}^{\mathrm{loc}} + \log\left[\prod_i\left(\frac{C_j}{C_j^{\mathrm{ref}}}\right)^{q_j}\right]\right) \tag{13}$$

Additionally the double-layer capacitance C_{d} affects the electric response of the fuel cell. The double-layer capacitance of the anode and cathode $C_{\mathrm{d,a,c}}$ were separately modelled with a feed-back loop using the following equation:

$$\frac{\mathrm{d}\eta_{\mathrm{a}}^i}{\mathrm{d}t} = \frac{i}{C_{\mathrm{d,a,c}}} = \frac{1}{R_{\mathrm{a,c}}C_{\mathrm{d,a,c}}}\left(\eta_{\mathrm{a,c}}^{i-1} - \eta_{\mathrm{a,c}}^i\right) \tag{14}$$

The model calculates the ohmic losses within the catalyst layer. Two sources of ohmic losses have been considered:

- The potential drop within the electrolyte solution defined by the solution conductivity.
- The voltage drop within the electrodes defined by the ohmic resistance of the solid electrode materials and the current collector.

The solution potential drop is described by

$$\Delta\Phi = \frac{i x_i}{\sigma} \tag{15}$$

The voltage drop within the catalyst solid material is described by Ohm's law:

$$\eta_{\mathrm{ohmic,a,c}} = \frac{i A_{\mathrm{FC}}}{\sigma_{\mathrm{a,c}} x_i} \tag{16}$$

As a consequence of the electric and electrochemical considerations the overall anode and cathode voltage was calculated from

$$E_{\mathrm{a,c}} = E_{\mathrm{a,c}}^{\mathrm{N}} + \eta_{\mathrm{a,c}} + \phi_{\mathrm{a,c}} + \eta_{\mathrm{ohmic,a,c}} \tag{17}$$

3.1.3. Electrolyte layer

Within the electrolyte layer there are no chemical reactions. Further, no gassing or dissolution of reaction species occurs, i.e. there is no mass transfer over the phase boundary. Five species exist within the layer: dissolved hydrogen, dissolved oxygen, water, hydroxyl anions and potassium cations. All species occur in the liquid phase. As can be seen from the simulation results, it is important to consider the change in electrolyte concentration

across the fuel cell, as the electrolyte concentration affects most model parameters.

In the model the electrolyte concentration in the middle of the electrolyte layer $C_{e\_2,5}$ was assumed to be constant and equals the reference concentration $C_{e,ref}$. The electrolyte concentrations at point 2 (C_{e_2}) and point 3 (C_{e_3}) were calculated using the continuity equation. No chemical reaction and transport over a phase boundary occurs in the electrolyte layer, hence the continuity equation consists only of Nernst–Plank transport term and has the following form:

$$\frac{\varepsilon^{\text{elec}}\,\mathrm{d}C_e}{\mathrm{d}t} = -\frac{\mathrm{d}N_e}{\mathrm{d}x} = \frac{\mathrm{d}\left(D^{l}_{K^+/H_2O}(\mathrm{d}C_e/\mathrm{d}x) + z_{K^+}Fu_{K^+}C_e(\mathrm{d}\Phi/\mathrm{d}x) + (\upsilon^{\text{ave}}C_e/\mathrm{d}x)\right)}{\mathrm{d}x} \tag{18}$$

Additionally the solution potential Φ was calculated in the electrolyte layer and is defined by

$$\Delta\Phi = \frac{ix_i}{\sigma}$$

3.1.4. Overall cell and stack potentials

The anode and cathode potentials E_a, E_c follow from the above considerations:

$$E_a = E_a^N - \Phi_a - \eta_a - \eta_{iR,a} \tag{19}$$

$$E_c = E_c^N - \Phi_c - \eta_c - \eta_{iR,c} \tag{20}$$

The overall single cell potential E_{cell} follows from the difference of cathode and anode potential:

$$E_{cell} = E_c - E_a \tag{21}$$

The model calculates the stack voltage E_{stack} by multiplying the simulated voltage of a single cell E_{cell} with the numbers of cells connected in series ($n_{series}n_{modules}$):

$$E_{stack} = E_{cell}n_{series}n_{modules} \tag{22}$$

The input load current I_{load} signal was divided by the number of cells connected in parallel in the stack $n_{parallel}$ to calculate the current demanded of a single cell I_{cell}:

$$I_{cell} = \frac{I_{load}}{n_{parallel}} \tag{23}$$

To take recognition of the ohmic losses caused by the interconnections the overall stack voltage is reduced by an ohmic voltage loss η_{inter}:

$$E_{stack,real} = E_{stack} - \eta_{inter} \tag{24}$$

4. Simulation results

Using the operating conditions listed in Table 1 the distribution of the main AFC parameters across a single cell were simulated and compared to test and literature data [3–5].

Table 1
Operating conditions of Zetek AFC stack

Parameter	Symbol	Value
Anode and cathode inlet gas pressures	p_a, p_c	1.053 atm
Reference electrolyte concentration	$C_{e,ref}$	6.6 M
Fuel cell temperature	T_{FC}	70 °C

4.1. Steady-state simulations

Fig. 4 shows the ideal voltage–current characteristic of a two-module Zetek stack compared with simulation results. The test data was supplied by the manufacturer. The data does not include information about the activation and concentration limitations, only the open circuit voltage of the stack is given (11.3 V).

It is clear from Fig. 4 that the simulation accurately describes the stack polarisation. The correlation factor R_{chi} was calculated to be 96.7% for the given data points. The overall stack resistance R_{stack} in the linear region (25–110 A) was calculated to be 25 mΩ. The limiting current for the stack determined by the model is 140 A (130 mA cm^{-2}). The open circuit voltage is calculated to be 11.3 V. The nominal operating voltage of the stack is 8 V (0.67 V per cell) which leads to a nominal stack current of 100 A. The generated electric power of the fuel cell stack relative to the stack current is also shown in Fig. 5. At the nominal operating current of 100 A the stack generates 800 W_e. After reaching a current of 125 A the concentration losses increase exponentially, due to the lack of reaction oxygen (as later shown). At a stack current of 140 A the voltage and consequently the power collapses. This is the point where the concentration of oxygen on the reaction interface equals zero.

Additionally the polarisation curve of a single cell of the Zetek AFC stack was investigated. The characteristics for anode, cathode and the overall single cell are shown in Fig. 6. The Zetek stack simulated consist of 24 cells connected in parallel (4 cells) and series (12 cells) fashion. Hence, the current of a single cell was calculated to be a quarter of the fuel cell stack current. The

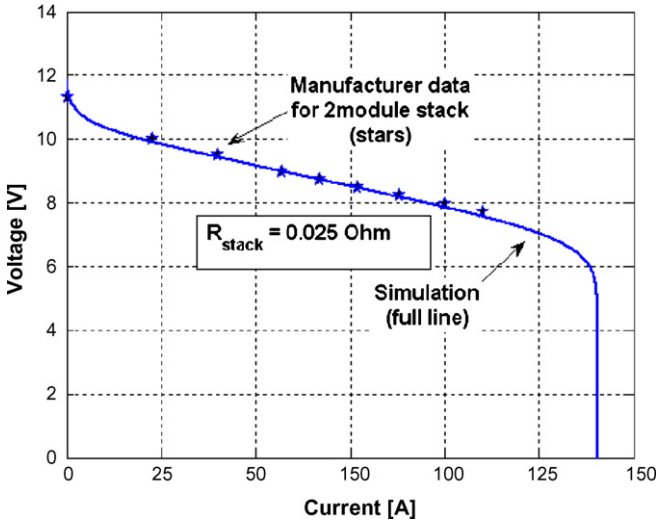

Fig. 4. Zetek AFC stack voltage–current characteristic, comparison between simulation results and manufacturer data.

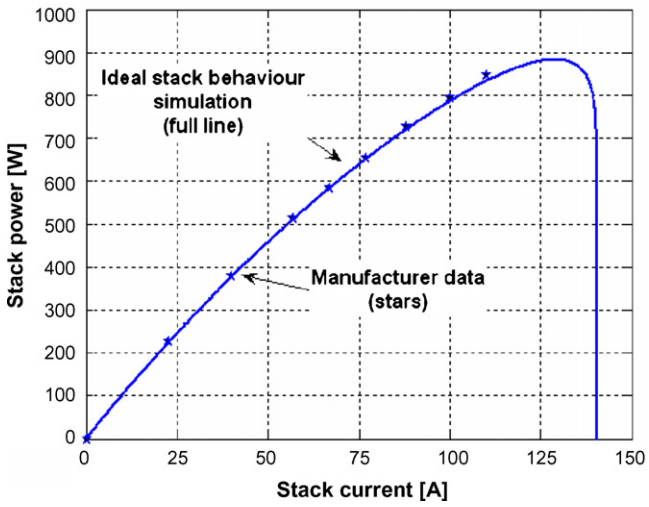

Fig. 5. Zetek AFC stack power–current characteristic, comparison between simulation results and manufacturer data.

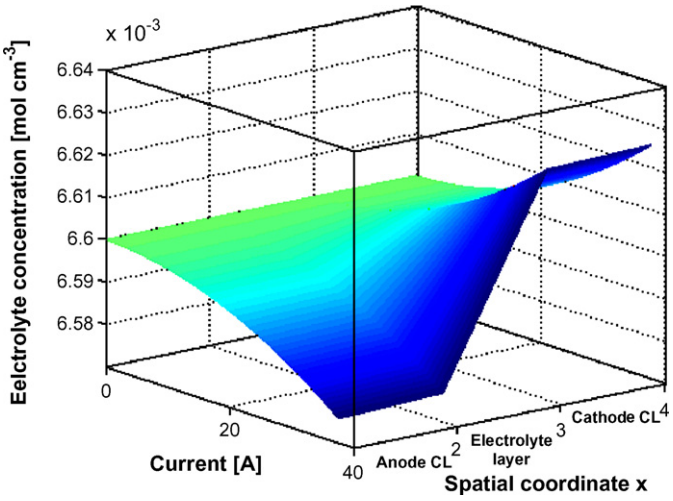

Fig. 7. Electrolyte concentration within the Zetek alkaline fuel cell as a function of current.

single cell open circuit voltage was calculated to be 0.94 V, which confirms the manufacturer data. The overall losses of the Zetek cell are principally determined by the cathode overpotential with a simulated limiting current density of 130 mA cm^{-2} (35 A for a single cell, 140 A for the stack).

Fig. 7 shows the electrolyte distribution throughout a single cell relative to the applied current. As expected the simulation shows that under open circuit conditions the electrolyte concentration is uniform throughout the three layers with a reference concentration of 6.6 M. When the load is applied the KOH concentration on the anode side decreases and C_e on the cathode side increases due to the chemical reactions on the electrodes. It can be seen that the main concentration drop occurs within the electrolyte layer, whereas within the anode and cathode catalyst layers the electrolyte concentration varies only slightly.

This effect can be explained by the fact that the electrolyte layer is 1000 times the thickness of the catalyst layers (electrolyte layer 1 mm, catalyst layers 0.001 mm). The simulation shows that it is important to take recognition of the variation in C_e. Thus, the electrolyte concentration has an important influence on a variety of fuel cell properties as previously highlighted.

The concentration profile of the dissolved hydrogen and oxygen within the catalyst layers and the electrolyte layer relative to the current are shown in Figs. 8 and 9. It is clear from Fig. 8 that even at the limiting current of 35 A for a single cell, sufficient amount of hydrogen can be provided to the reaction area. The hydrogen concentration drops to a minimum of 0.9×10^{-7} mol cm^3 in the catalyst layer. It has been assumed that hydrogen travelling through the electrolyte to the cathode will immediately react on the interface. Hence, the hydrogen concentration on the electrolyte–cathode catalyst layer interface equals zero.

Fig. 9 illustrates that at higher currents the oxygen concentration is substantially reduced. At the limiting current I_l 35 A ($i_l = 0.13$ A cm^{-2}) the concentration of dissolved oxygen in the catalyst drops to zero and consequently any further load increase will lead to the collapse of the fuel cell voltage.

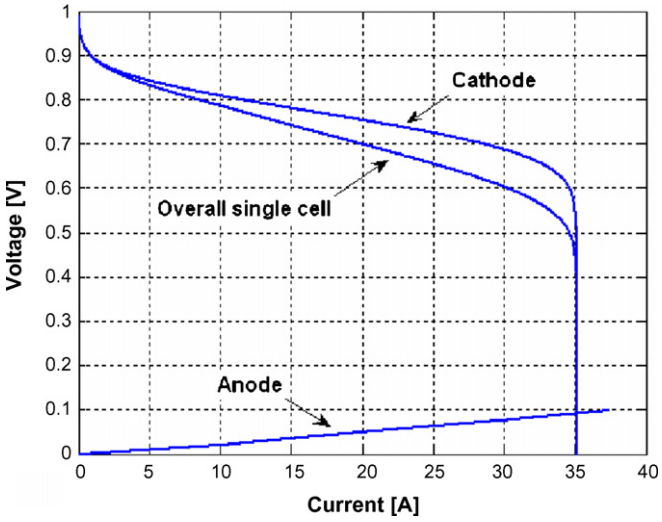

Fig. 6. Voltage–current characteristics of anode, cathode and single cell.

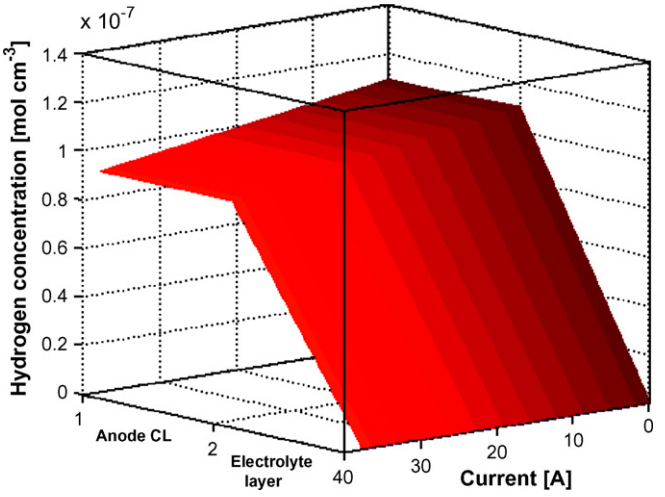

Fig. 8. Dissolved hydrogen concentration profile within the alkaline fuel cell as a function of current.

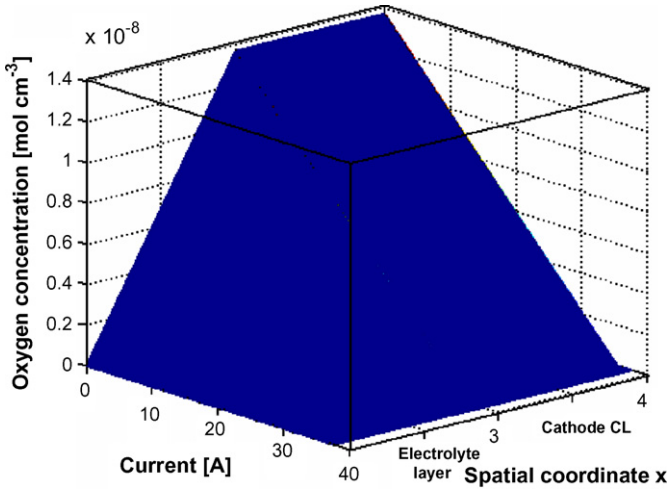

Fig. 9. Dissolved oxygen concentration profile within the alkaline fuel cell as a function of current.

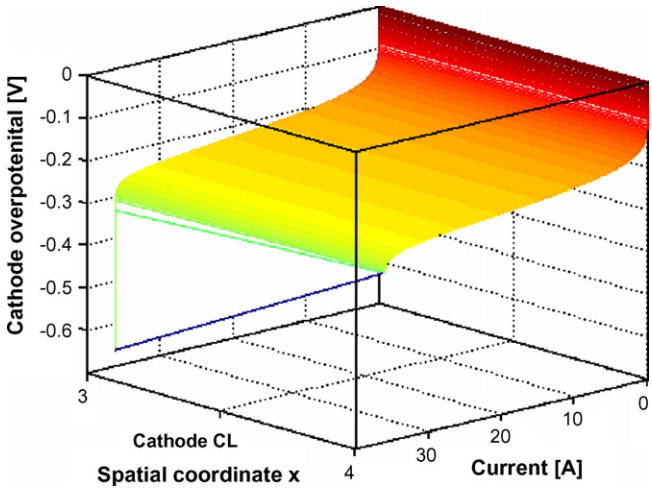

Fig. 11. Cathode overpotential profile as a function of current.

In Figs. 10 and 11 the anode and cathode overpotentials (activation and concentration losses) are shown, respectively. The positive sign of the anode overpotential results from the fact that the Nernst potential of the anode is positive (0.3 V) at the given operating conditions, whereas the cathode Nernst potential is negative (−0.8 V). The higher overpotential on the cathode is the result of its oxygen mass transport limitations and lower exchange current density.

As expected (see also Fig. 6) the cathode overpotential is much larger than the anode overpotential and consequently the cathode overpotential is the performance-dominating factor. It is shown that the total anode overpotential is very small, with its maximum at 35 A of 0.027 V. Due to the preferable hydrogen oxidation process on the anode the activation overpotential at low current (until 10 V) is calculated with the model to be zero. This shows that at limiting current (35 A) there is still enough dissolved hydrogen in the catalyst layer to keep the oxidation process going. The overpotential on the cathode reaches a maximum of −0.35 V at the limiting current. At low current (0–5 A) the activation polarisation is dominant, whereas at a current over 30 A the concentration polarisation causes an exponential increase of the losses. The figure also illustrates, that the model predicts a collapse of the fuel cell voltage for a current higher than 35 A through a dramatic increase in the cathode overpotential.

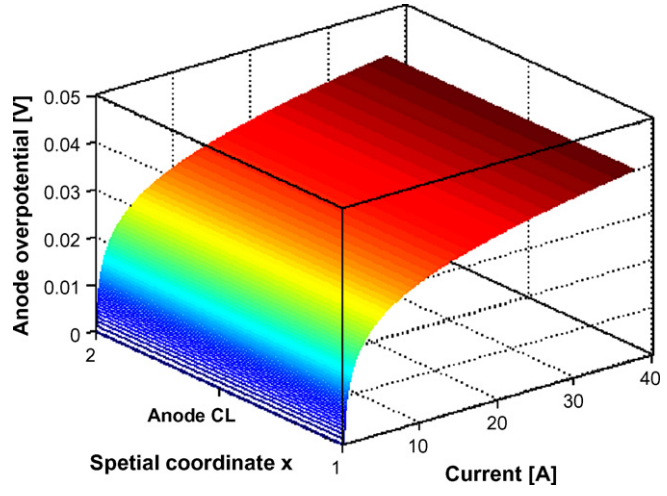

Fig. 10. Anode overpotential profile as a function of current.

4.2. Dynamic load switching simulations

Figs. 12 and 13 show the voltage and current responses of the fuel cell stack from open circuit to an applied resistive load of 0.558 Ω, respectively. Both figures compare the test results with the simulated dynamic behaviour of the stack.

The open circuit voltage of the stack at the beginning of the test was measured to be 10.7 V. After 0.5 s the resistive 0.558 Ω load was applied. Immediately following the application of the load the voltage drops due to the internal resistance of the stack. The exponential decay which follows is caused by a combination of mass transport dynamics and the partial discharge of the electric double layer. The final steady-state voltage level of the stack

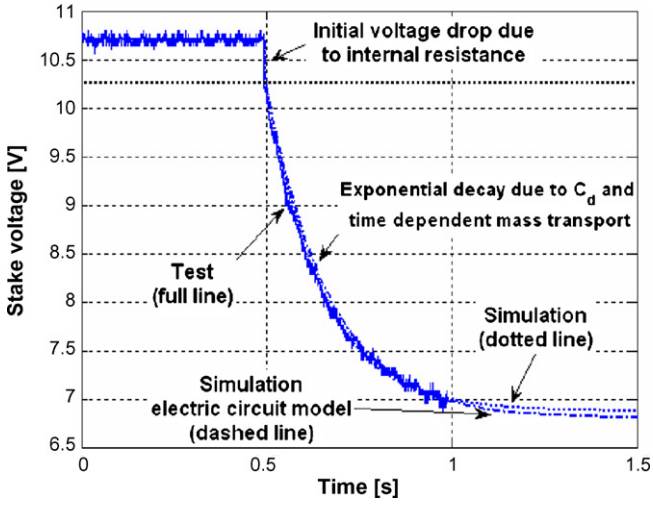

Fig. 12. Voltage–time characteristic, comparison between test data and simulation results for load switching of a 0.558 Ω resistive load.

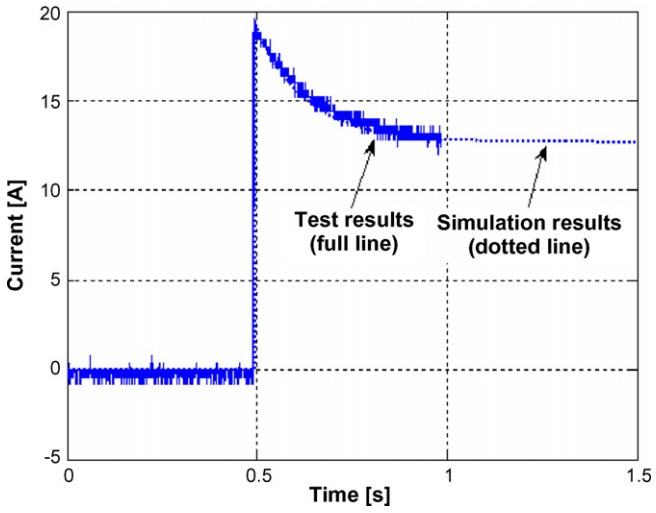

Fig. 13. Current–time characteristic, comparison between test data and simulation results for load switching of a 0.558 Ω resistive load.

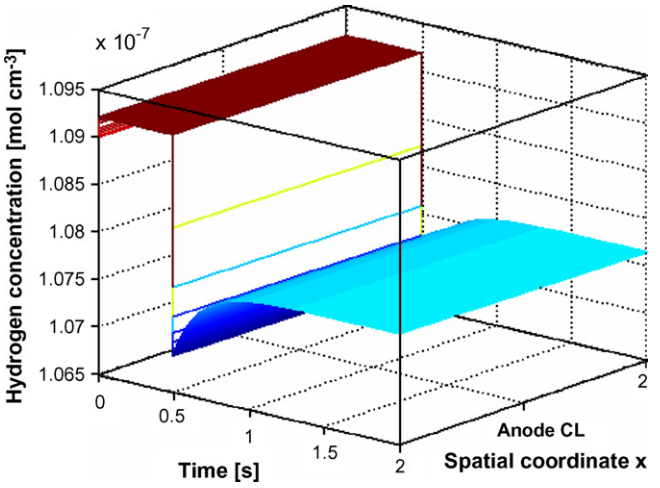

Fig. 15. Dissolved hydrogen concentration profile for load switching of a 0.558 Ω resistive load.

is reached after approximately 1 s and is 6.8 V. The test started at open circuit. Directly after the load is applied the current rises to 19.8 A due to the discharge of some stored electric energy within the double-layer capacitance structure. Within approximately 1 s after switching the stack current decreases exponentially to a steady-state current value of 13.2 A. The model accurately predicts the transient behaviour of the 0.558 Ω resistive load switching test with calculated correlation factors R_{chi} of 98.5% for the voltage transient simulation and an R_{chi} value of 98.2% for the current transient simulation.

To investigate the effects of the load switch on the fuel cell internal behaviour some parameters were investigated in more detailed. The electrolyte concentration has an influence on a variety of fuel cell parameters and properties. Hence, was investigated to determine the changes across the fuel cell during the load switching event. Fig. 14 shows the electrolyte concentration across the anode CL, the electrolyte layer and the cathode CL. At the beginning of the test the fuel cell operates at open circuit and the electrolyte concentration is constant throughout the liquid layers at 6.6 M. After the load was applied the electrolyte concentration changed relative to the fuel cell current. On the anode the concentration decreases due to the production of water, whereas on the cathode the concentration increases due to the increase of hydroxyl ions.

Fig. 14 shows that the change in electrolyte concentration for the simulated switching test of 0.558 Ω is minimal. On the anode and cathode the maximum change is calculated to be 4×10^{-7} mol cm^3 (4×10^{-4} M). However, a comparison with Fig. 7 shows that the simulated electrolyte concentrations have not reached their steady-state values for the applied current of 13.2 A.

The steady-state change of the electrolyte concentration is approximately 10 times (4×10^{-6} mol cm^3) larger than the value of Fig. 14. The reason of this difference is caused by the slow mass transport within the electrolyte layer.

In Figs. 15 and 16 the concentration profiles of dissolved hydrogen and dissolved oxygen in the anode and cathode catalyst layers during load switching are shown, respectively.

After the load is applied at 0.5 s the concentration drops from 1.093×10^{-7} to 1.068×10^{-7} mol cm^{-3} and after a further 1 s

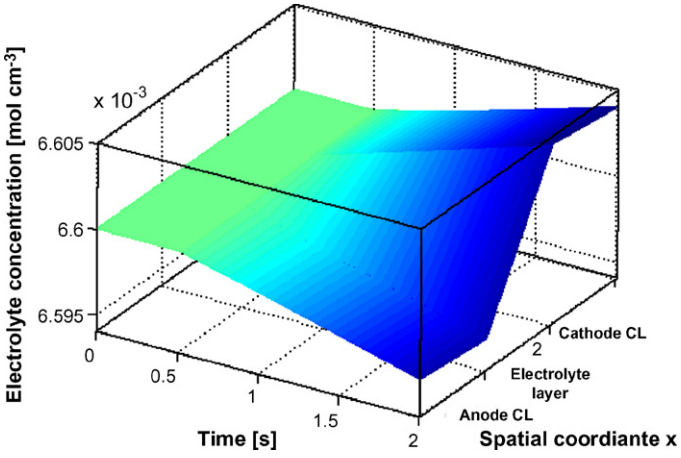

Fig. 14. Electrolyte concentration profile for load switching of a 0.558 Ω resistive load.

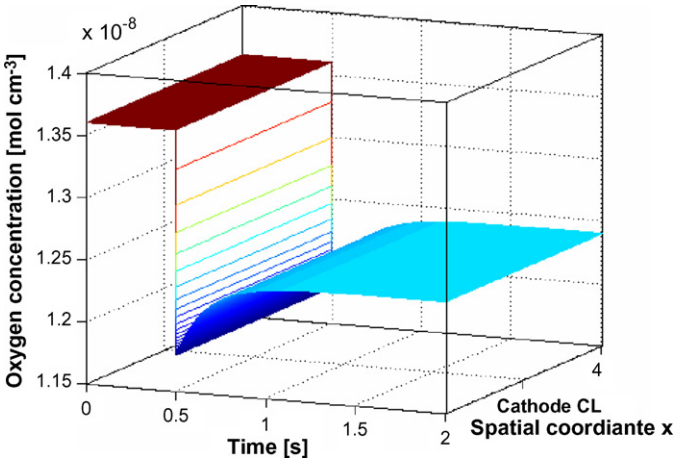

Fig. 16. Dissolved oxygen concentration profile for load switching of a 0.558 Ω resistive load.

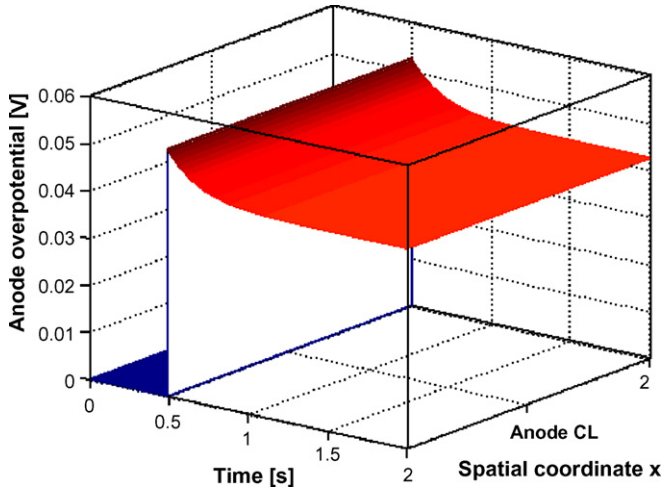

Fig. 17. Anode overpotential of a single cell for load switching of a 0.558 Ω resistive load.

adjust to its new steady-state value of 1.076×10^{-7} mol cm^{-3}. The initial concentration drop is caused by the higher reaction rate of oxygen during transient times and is a direct result of the current spike shown in Fig. 13. The oxygen concentration shows a similar behaviour as C_{H_2}. However, due to the smaller amount of oxygen used in the reaction the absolute oxygen concentration drop is smaller (1.1×10^{-9} mol cm^{-3}) compared with the C_{H_2} drop (1.7×10^{-9} mol cm^{-3}). Also it must be noticed that the amount of dissolved oxygen (1.36×10^{-8} mol cm^{-3}) is approximately eight times smaller than the amount of dissolved hydrogen (1.093×10^{-7} mol cm^{-3}) on open circuit. The reason is as explained before is the lower solubility of oxygen in the electrolyte.

Figs. 17 and 18 show the anode and cathode overpotentials caused by the activation and concentration losses, respectively. Both overpotentials are zero at the beginning of the load switching simulation, as the fuel cell is operating at open circuit. After the load is applied the overpotentials rise immediately mainly due to the experienced concentration limitations. It is shown in Fig. 17 that the simulation predicts a relative small value for the anode overpotential of 0.042 V after the load switching, whereas the overpotential of the cathode increases sharply to −0.26 V for a single cell (see Fig. 18). The anode and cathode overpotentials of the stack were simulated to be 0.126 and −0.78 V, respectively, for the test stack.

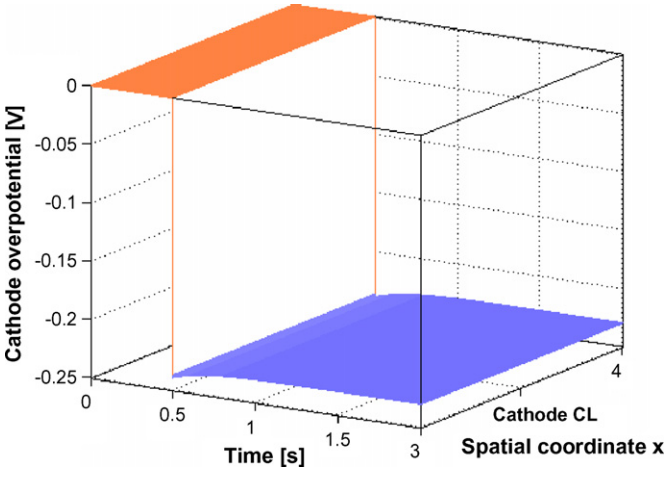

Fig. 18. Cathode overpotential of a single cell for load switching of a 0.558 Ω resistive load.

5. Conclusions

The dynamic model forecasts the steady-state and dynamic behaviour of the alkaline fuel cell stack. The effects of the load changes on various fuel cell parameters, such as electrolyte concentration and concentrations of dissolved hydrogen and oxygen were covered in this investigation. The author's model considers the main loss effects of an AFC; the activation, ohmic and concentration losses. The dynamics behaviour of the fuel cell process was modelled through dynamic mass balances of the reactant species and through the consideration of the double-layer capacitance. A comparison of simulation results with manufacturer and test data has shown the accuracy of the model.

The model will be part for a larger hybrid fuel cell/battery system model and is also the basis for the development of an AFC condition-monitoring unit.

Appendix A. List of symbols

a^{g}	specific area of gas–electrolyte interface (cm^2 cm^{-3})
a^{l}	specific area of catalyst–electrolyte interface (cm^2 cm^{-3})
A_{FC}	area of the cell (cm^2)
$C_{d,a,c}$	double-layer capacitance of anode and cathode (F)
C_i	concentration of species i in electrolyte solution (mol cm^{-3})
C_i^{ref}	reference concentration of specie i (mol cm^{-3})
D_i^{l}	diffusion coefficient of species i in liquid phase (cm^2 s^{-1})
D_{ij}	gas diffusion coefficient of species i in j (cm^2 s^{-1})
$E_{a,c}$	anode and cathode potential (V)
$E_{a,c}^{N}$	anode and cathode Nernst potential (V)
$E^{N,0}$	Nernst or open circuit potential at standard conditions (V)
F	Faraday constant (96 485 C mol^{-1})
H_i	Henry constant for species i (mol cm^{-3} bar^{-1})
i	current density (A cm^{-2})
i^{loc}	anodic and cathodic local current density (A cm^{-2})
i_0^{loc}	anodic and cathodic local exchange current density (A cm^{-2})
N_i	molar flux of species i (mol cm^{-2} s^{-1})
N_i^{l}	molar flux of species i in liquid phase (mol cm^{-2} s^{-1})
p	total pressure (bar)
p_i	partial pressure of species i (mol cm^{-3})
$q_{i,j}$	reaction order of species i, j
R	universal molar gas constant (8.31451 J mol^{-1} K^{-1})
$R_{a,c}$	anode and cathode ohmic resistance (Ω)
R_i^{e}	chemical reaction rate of species i (mol cm^{-3} s^{-1})

R_i^{p} mass transport rate over phase boundary of species i ($\mathrm{mol\,cm^{-3}\,s^{-1}}$)
s_i stoichiometric coefficient of species i
T temperature (K)
u_i effective mobility of species i ($\mathrm{mol\,cm^2\,J^{-1}\,s^{-1}}$)
x_i thickness of layer i
y_i vapour mole fraction of species i
z_i number of electrons involved in reaction

Greek letters

$\alpha_{\mathrm{a,c}}$ anodic and cathodic transfer coefficient for reaction
δ thickness of electrolyte film (cm)
$\varepsilon^{\mathrm{GDL}}$ porosity of the GDL
$\eta_{\mathrm{a,c}}$ anode and cathode overpotential (V)
$\eta_{\mathrm{a,c}}^{i}$ anode and cathode overpotentials at present time (V)
$\eta_{\mathrm{a,c}}^{i-1}$ anode and cathode overpotentials at last time step (V)
$\eta_{i\mathrm{R,a,c}}$ anode and cathode ohmic losses (V)
$\eta_{\mathrm{ohmic,a,c}}$ anodic and cathodic voltage drop (V)
υ^{ave} volume average velocity ($\mathrm{cm\,s^{-1}}$)
$\sigma_{\mathrm{a,c}}$ effective anodic and cathodic conductivity ($\mathrm{S\,cm^{-1}}$)
$\Phi_{\mathrm{a,c}}$ anode or cathode solution potential (V)

References

[1] E&G Technical Services, Inc., Fuel Cell Handbook, 7th ed., U.S. Department of Energy, Office of Fossil Energy, November 2004, ISBN 1-41021-960-7.
[2] J.-H. Jo, S.-C. Yi, A computational simulation of the alkaline fuel cell, J. Power Sources 84 (1999) 87–106.
[3] Zetek Power Plc., Design Guidelines for the ZeTek Power Alkaline Electro-Chemical Generator, internal report, Doc No. 01001-12-00, Scottish Fuel Cell Consortium, December 2000.
[4] T. Burchardt, P. Gouerec, E. Sachez-Cortezon, Z. Karichev, J.H. Miners, Alkaline fuel cells: contemporary advancement and limitations, Fuel 81 (2002) 2151–2155.
[5] C. Wilson, A. Davidson, B. Brownlee, Zetek Module component analysis and characterisation, Internal Report, University of Strathclyde, EEE Department, Glasgow, 2004.